A novel cool material: ASA (acrylonitrile-styrene-acrylate) matrix composites with solar reflective inorganic particles

Bo Xiang [a, b], Xiuping Yin [a, b], Jun Zhang [a, b, *]

[a] College of Materials Science and Engineering, Nanjing Tech University, Nanjing 210009, China
[b] Jiangsu Collaborative Innovation Center for Advanced Inorganic Function Composites, Nanjing 210009, China

ARTICLE INFO

ABSTRACT

Nowadays, the undesirable heat generated from solar energy troubles people a lot in various aspects, including the energy consumption for cooling purposes, the potential safety hazards of the outdoor devices used in high-temperature environment and so on. Therefore, many cool materials emerge as the times require, which can mitigate these serious situation. In this study, a concept of solar reflective ASA (acrylonitrile-styrene-acrylate terpolymer) for cool material was proposed. To achieve this purpose, several inorganic particles with high solar reflectance were chosen to mix with ASA via melt blending to improve the cooling property of ASA. Ultraviolet-visible-near infrared (UV-Vis-NIR) spectral and temperature test were carried out to evaluate the cooling properties of ASA and its hybrid composites. The results of the solar spectral test showed that the addition of only 1% volume fraction of inorganic particles could effectively improve the solar reflectance of ASA. And ASA/barium titanate (BaTiO$_3$) hybrid composite possessed the highest reflectance value of 67.66%, nearly 2 times that of neat ASA. The results of the indoor temperature test were in highly consistent with those of the solar reflectance, which showed that all the hybrid composites presented better cooling effect compared with neat ASA. Also, ASA/BaTiO$_3$ hybrid composite exhibited the best cooling effect, nearly 10 °C lower than neat ASA. Besides, the outdoor temperature test showed the same trend with the indoor temperature test. Furthermore, the results of the mechanic test indicated that the improvement of the cooling properties was based on no sacrifice of the mechanical properties.

1. Introduction

Among all the renewable energy sources, solar energy has attracted more attentions as it has resource potential that far exceeds the entire global energy demand [1]. Hence, solar energy has delivered a great contribution to the solution of human's energy problem [2]. However, the solar energy also troubles people a lot in various aspects as solar radiation may generate undesirable heat, especially in hot summer. For instance, the high temperature caused by the undesirable heat inside buildings and cars brings people uncomfortable feelings. Besides, the refrigerated foods (fresh meat, egg and milk, etc.) may go bad due to the undesirable heat during transportation by truck [3]. Although the use of the cooling equipment can mitigate these situations, amounts of unnecessary energy consumption are generated [4]. For another instance, the use of outdoor devices, such as base station antenna, in high-temperature environment may cause some potential safety hazards. Thus, housings with cooling property for outdoor devices are essential. To solve these troubles, many cool materials emerge as they can decrease the heat built-up and minimize the temperature rise. Song et al. [5] used titanium dioxide rutile pigments to improve the solar reflectance of cool non-white coatings and an approximately 15% improvement of the integrated solar reflectance could be obtained. Soumya et al. [6] used solution mixing method to prepare poly(methyl methacrylate) (PMMA)/Zinc oxide (ZnO) composites and the near infrared reflectance at the wavelength of 810 and 1100 nm could be significantly increased to 55 and 53%, respectively. Raj et al. [7] synthesized a new class of pigments with high near infrared (NIR) reflectance (80% at 1100 nm) as potential NIR reflective candidates for cool roof and surface coating applications. Besides, Lu et al. [8] manufactured a novel energy efficiency roof coupled with phase change materials and cool materials which could effectively improve the indoor thermal environment and

* Corresponding author. College of Materials Science and Engineering, Nanjing Tech University, Nanjing 210009, China.
E-mail address: zhangjun@njtech.edu.cn (J. Zhang).

lower air conditioning load evidently. All these works have made tremendous contribution to the field of cool material and effectively reduced the unnecessary energy loss. And based on these works, more meaningful research, such as the study of other new solar heat-reflective pigments or new matrix for cool material, could also be carried out to promote the development of cool material.

Acrylonitrile-styrene-acrylate terpolymer (ASA) has a similar core-shell structure with acrylonitrile-butadiene-styrene terpolymer (ABS) except that the butadiene rubber was replaced by acrylate rubber, which can alleviate the physical (or chemical) aging of butadiene rubber by removing the degradation of C=C double bond in the backbone of ABS [9]. Therefore, ASA has more excellent weather resistance property. Besides, the unique core-shell structure gives ASA many other excellent properties, such as high toughness, good dimensional stability, well thermal stability as well as excellent mechanical properties. These excellent properties make ASA suitable for various outdoor applications [10]. However, the solar reflectance of ASA is not very high, which means a poor cooling property. Therefore, it will be a meaningful work to improve the cooling property of ASA. Mixing polymer matrix with inorganic solids to prepare organic/inorganic composite is a common and easy-to-perform polymeric modification method, which can obtain significant improvement of physical and/or chemical properties over the matrix polymers [11,12].

In our previous work, titanium dioxide (TiO_2) was used to improve the cooling property of high density polyethylene (HDPE) and the total solar reflectance could be increased to 65.2% [13]. On one hand, it may be ascribed to the influence of TiO_2 on the crystallization behavior of HDPE. On the other hand, the high solar reflectance of TiO_2 particles is indispensable. Based on this, six kinds of inorganic particles with high solar reflectance were chosen to mix with ASA to improve the cooling property of ASA. And some of them have even not been used as solar reflective pigment for cool material so far, such as barium titanate ($BaTiO_3$) which was extensively used in manufacturing electronic materials [14,15]. Then, solar reflective ASA for cool material would be obtained.

2. Design concept

The schematic diagram for our design concept of solar reflective ASA is illustrated in Fig. 1. In the figure, the inorganic particle-1 is able to reflect full-band sunlight reaching the earth's surface, while the inorganic particle-2 can reflect visible and near-infrared band but absorb ultraviolet band sunlight reaching the earth's surface. Two kinds of ideal solar reflective ASA were proposed. One is solar reflective ASA-I consisting of ASA and inorganic particle-1, which can reflect full-band sunlight as shown in Fig. 1c. The other one is solar reflective ASA-II consisting of ASA and inorganic particle-2, which can reflect visible and near-infrared band but absorb ultraviolet band sunlight as shown in Fig. 1d.

In fact, we are more inclined to solar reflective ASA-II and there are mainly two reasons. Firstly, the high-energy ultraviolet light usually leads to the degradation of polymers [16]. If the inorganic particles can absorb most of the ultraviolet light, the polymer around the particles will share little and avoid being damaged. Then, the anti-ultraviolet ageing performance of the polymer will be improved dramatically. Secondly, although the energy of ultraviolet light is very high, its wavelength range (from 280 to 400 nm) is too narrow. And the ultraviolet light occupies only about 5% of the total radiation reaching the earth's surface [16]. Therefore, the absorption of ultraviolet light will have little influence on the cooling property of solar reflective ASA.

3. Experimental

3.1. Materials

ASA (HX-960, density = 1.05 g/cm^3) was supplied by Zibo Huaxing additives Co., Ltd., China. ZnO (density = 5.61 g/cm^3) was a product from Nanjing Chemical Material Corp., Ltd., China. Calcium molybdate ($CaMoO_4$, density = 4.35 g/cm^3) was made by ourselves. Yttrium oxide (Y_2O_3, density = 5.01 g/cm^3) was purchased from Beijing Founde Star Science & Technology Co., Ltd., China. TiO_2 (density = 4.25 g/cm^3) was commercially obtained from Xuancheng Jingrui New Material Co., Ltd., China. Antimony oxide (Sb_2O_3, density = 5.67 g/cm^3) was received from Yiyang Huachang Antimony Industry Co., Ltd., China. $BaTiO_3$ (density = 6.02 g/cm^3) was supplied by Foshan Songbao Electronic Functional Material Co., Ltd., China.

3.2. Sample preparation

ASA was mixed with the inorganic particles in a two-roll mill (SK-160B, Shanghai Rubber Machine Factory, China) at 180 °C. Since the densities of the inorganic particles are different to each other, the addition amount of the inorganic particles was set to a volume fraction of 1%. The detailed formulation of different samples is defined in Table 1. After the melt blending, the prepared blends were compression-molded into approximately 1 mm, 2 mm, and 4 mm thickness sheets at 180 °C. The sheets of approximately 1 mm thickness were prepared for ultraviolet-visible-near infrared (UV-Vis-NIR) spectral and temperature test. The dumb-bell shaped pieces cut from 2 mm sheets were used for tensile tests. The 4 mm sheets were machined into rectangular samples ($80 \times 10 \times 4$ mm^3) for impact and flexural tests.

3.3. Characterization

3.3.1. Wide angle X-ray diffraction (WAXD) measurement

In order to determine the actual phase composition of the inorganic powders, WAXD measurement was performed by a Rigaku Smart Lab 3000 diffractometer, operating with Cu K_α radiation (35 kV, 30 mA). The scanning velocity and range were 10°/min and 10°−80°, respectively.

3.3.2. Fourier transform infrared (FTIR) spectra analysis

The inorganic powders were also tested by FTIR spectra. And the spectral curves were measured using a FTIR spectrometer (Nexus 670, Nicolet, USA). Each spectrum was collected at the resolution of 4 cm^{-1} in the range of 4000−400 cm^{-1}.

3.3.3. UV-Vis-NIR spectral measurement

The UV-Vis-NIR reflectance spectra were measured by a spectrometer (Shimadzu UV-3600, Japan) with an integrating sphere. The scanning spectral region was from 200 to 2600 nm. Barium sulfate was applied as the white reference. Each spectrum reported is an average of three spectra recorded in different areas of the sample. Here, the reflected fraction $R_{\lambda_0 \to \lambda_1}$ of solar irradiation incident at wavelength between λ_0 and λ_1 is defined as the irradiance-weighted average of its spectral reflectance $r(\lambda)$, and it can be calculated using the following equation [17]:

$$R_{\lambda_0 \to \lambda_1} = \left[\int_{\lambda_0}^{\lambda_1} r(\lambda)i(\lambda)d\lambda \right] \Big/ \left[\int_{\lambda_0}^{\lambda_1} i(\lambda)d\lambda \right] \tag{1}$$

where $i(\lambda)$ represents the solar spectral irradiance (energy per unit
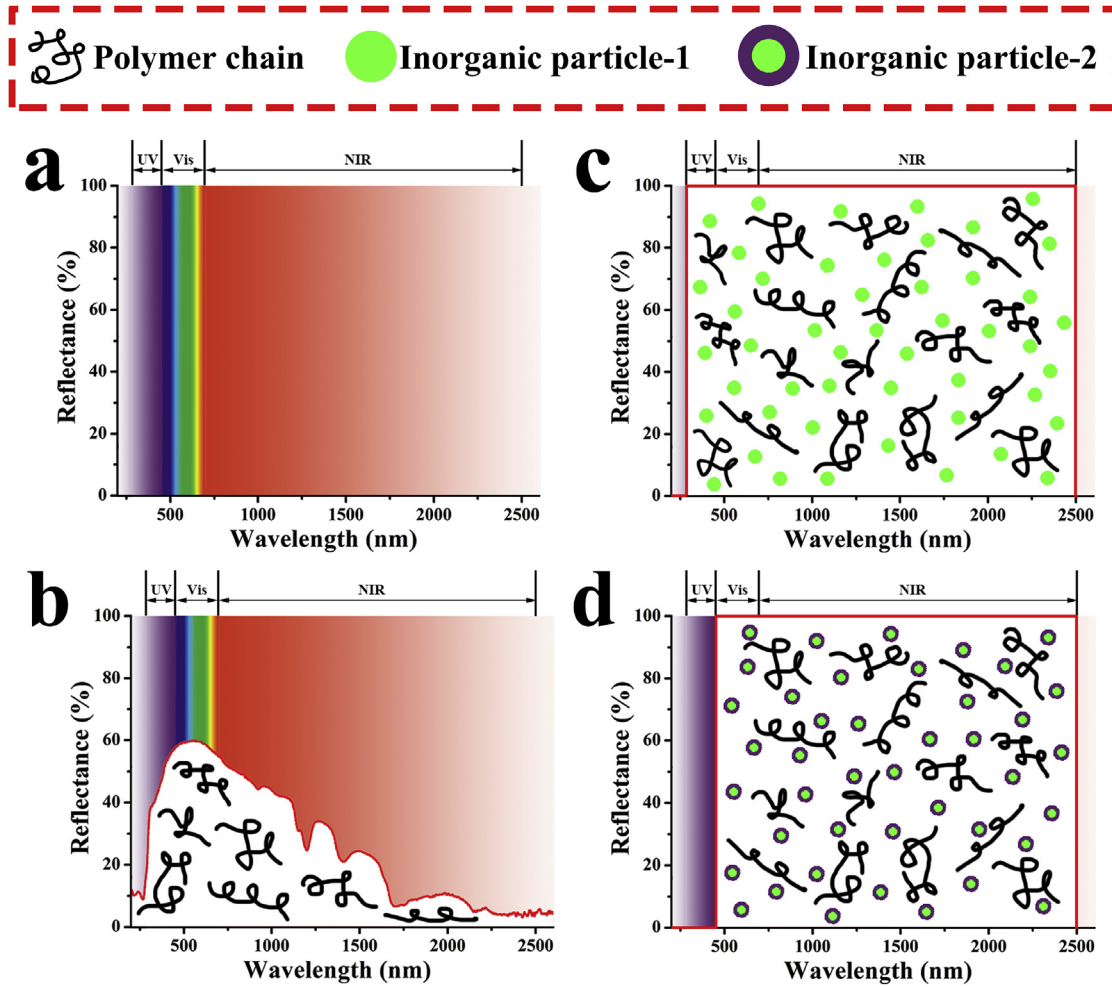
Fig. 1. Schematic diagram for our design concept of solar reflective ASA: (a) spectrum of sunlight reaching the earth's surface, (b) solar reflectance of original ASA, (c) solar reflectance of ideal solar reflective ASA-Ι, (d) solar reflectance of ideal solar reflective ASA-ΙΙ.

Table 1
Formulation of samples blended with different inorganic particles.

Samples	Composition/g						
	ASA	ZnO	CaMoO₄	Y₂O₃	TiO₂	Sb₂O₃	BaTiO₃
ASA	208.0	–	–	–	–	–	–
ASA/ZnO	208.0	11.2	–	–	–	–	–
ASA/CaMoO₄	208.0	–	8.7	–	–	–	–
ASA/Y₂O₃	208.0	–	–	10.0	–	–	–
ASA/TiO₂	208.0	–	–	–	8.5	–	–
ASA/Sb₂O₃	208.0	–	–	–	–	11.3	–
ASA/BaTiO₃	208.0	–	–	–	–	–	12.0

area per unit wavelength).

The total solar reflectance R_{sol} (280–2500 nm) can be divided into three parts, respectively are UV reflectance R_u (280–400 nm), visible reflectance R_v (400–700 nm), and NIR reflectance R_n (700–2500 nm). And the total solar reflectance can be calculated by the following equation based on the distribution of each solar energy (5% UV, 43% visible, and 52% NIR) yield [17],

$$R_{sol} = 0.05R_u + 0.43R_v + 0.52R_n \qquad (2)$$

3.3.4. Temperature test

To evaluate the real cooling property of the composites, a sandwich structure device was designed by ourselves [18]. There are two different temperature test methods. One is indoor temperature test, which is performed with the assistance of a solar simulator (Solar 3A, Newport, America) as shown in Fig. 2. The light intensity at the surface of test sample is 0.3 W/cm² and the internal temperature of the device is read during a certain time interval. The test was conducted in a room with a constant temperature of about 20 °C. The other is outdoor temperature test, which is conducted in a sunny day at noon (from 12:45–13:45). All the test devices were placed on a piece of insulating foam to isolate the heat exchange between the devices and the ground. Also, the internal temperature of the device is read during a certain time interval.

3.3.5. Mechanical properties

The impact strength was measured by an Izod impact tester (UJ-4, Chengde Machine Factory, China) at room temperature, according to ISO 180. The tensile and flexural properties were tested by a universal testing machine (CMT 5254, Shenzhen SANS testing machine Co., Ltd., China) with steady rate of 5 mm/min for tensile test and 2 mm/min for flexural test according to ISO 527 and ISO 178, respectively. Each datum in the figure is the average value of at least three tests.
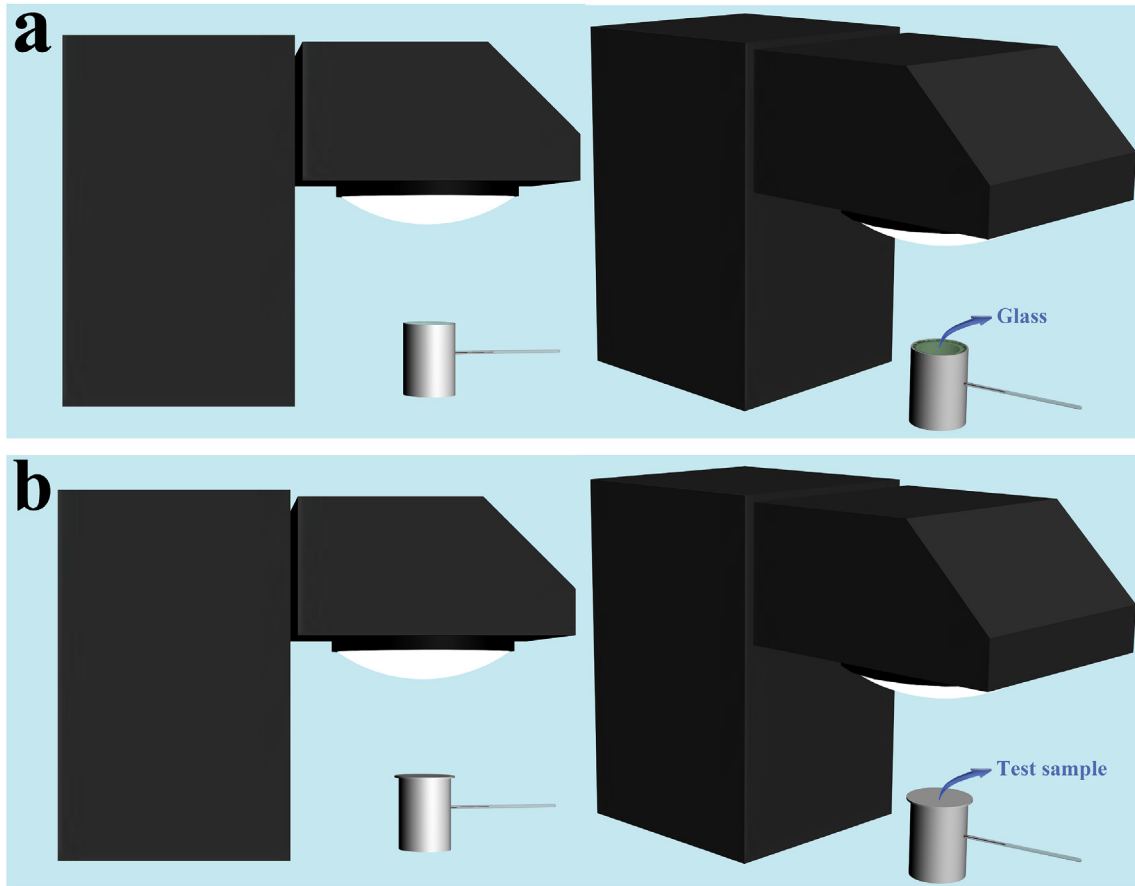
Fig. 2. Schematic diagram for the indoor temperature test: (a) tested with glass, (b) tested with sample.

4. Results and discussion

4.1. Characterizations of inorganic particles

4.1.1. WAXD analysis

WAXD diffraction patterns of different inorganic particles in the range 10–80° are sketched in Fig. 3. Through a series of comparison, it can be found that the patterns of the six inorganic particles are all well coincidence with the standard JCPDS cards (No. 36-1451 for wurtzite ZnO [19], No. 29-0351 for tetragonal $CaMoO_4$ [20], No. 05-0574 for cubic Y_2O_3 [21], No. 4-551 for rutile TiO_2 [22], No. 42-1466 for Sb_2O_3 [23] and No. 5-626 for tetragonal $BaTiO_3$ [24]).
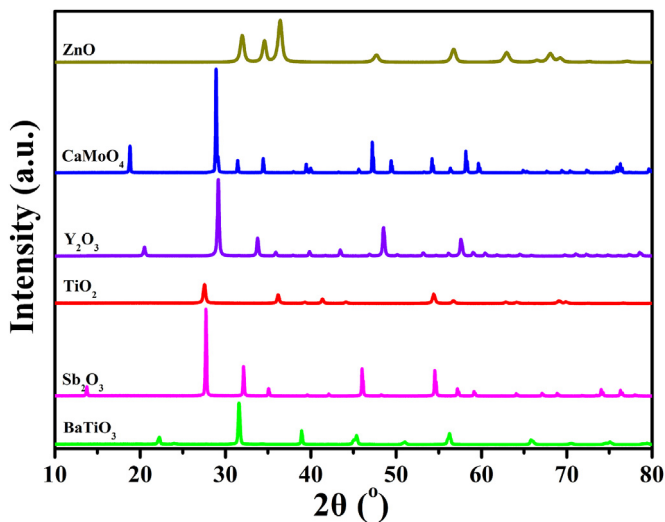

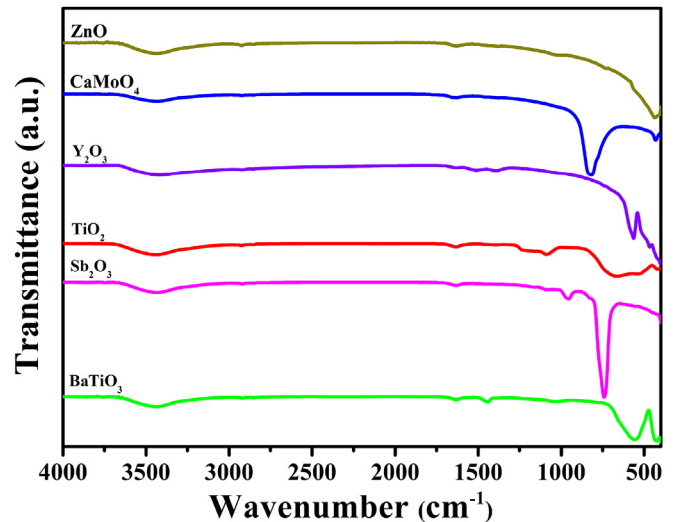**Fig. 3.** WAXD patterns of different inorganic particles.

Fig. 4. FTIR spectra of different inorganic particles.

4.1.2. FTIR analysis

The results of FTIR test are displayed in Fig. 4. Overall, the broad band between 3100 and 3700 cm^{-1} on all the six curves corresponds to the symmetric and asymmetric stretching vibrations of weakly bound water interacting with its environment via hydrogen bonding as well as the stretching vibrations of hydrogen-bonded OH groups. Moreover, on ZnO curve, the band located at about 440 cm^{-1} is diagnostic of ZnO [25]. On CaMoO$_4$ curve, the bands at 825 and 432 cm^{-1} are assigned to asymmetric stretching and bending vibrations of MoO$_4^{2-}$ tetrahedron, respectively [26]. On Y$_2$O$_3$ curve, the bands at 470 and 566 cm^{-1} are due to Y—O stretching vibrations [27]. On TiO$_2$ curve, the broad absorption in 400–800 cm^{-1} were assigned to Ti—O vibrations in TiO$_2$ [28]. On Sb$_2$O$_3$ curve, the two absorption bands at 740 and 960 cm^{-1} correspond to symmetric stretching and overtone vibrations of cubic Sb$_2$O$_3$, respectively [29]. On BaTiO$_3$ curve, the broad band at about 530 cm^{-1} is typical of the Ti—O vibrations in BaTiO$_3$ [30].

4.1.3. Solar reflectance

The solar reflectance of the inorganic particles is shown in Fig. 5. Obviously, compared with neat ASA, all the six kinds of inorganic particles have much higher solar reflectance, which indicates that these particles are able to improve the solar reflectance of ASA. Besides, a closer look at the reflectance curves can also reveal that CaMoO$_4$, Y$_2$O$_3$ and Sb$_2$O$_3$ can be classified as the inorganic particle-1 mentioned in Fig. 1. Because these three particles can reflect almost full-band sunlight as shown in Fig. 5. Of course, the remaining three particles including ZnO, TiO$_2$ and BaTiO$_3$ are classified as the inorganic particle-2 for they can reflect visible and near-infrared band but absorb ultraviolet band sunlight as illustrated in Fig. 5.

Through the above three characterizations, it can be confirmed that these six kinds of inorganic particles could be used for the next experimental research.

4.2. Cooling properties of ASA and its hybrid composites

4.2.1. Solar reflectance

After sample preparation, the optical property of all the samples was firstly tested. The solar reflectance is a very important property for cool materials which can indirectly reflect the cooling efficiency. Fig. 6 shows the solar reflectance of ASA and its hybrid composites.
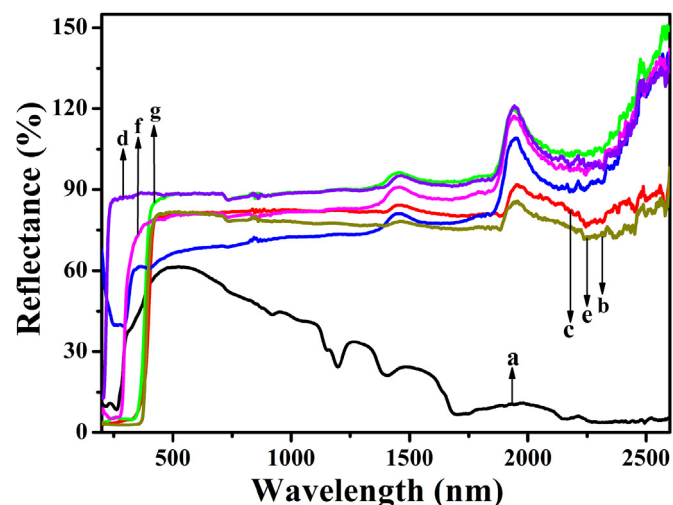

Fig. 5. Solar reflectance of ASA and different inorganic particles: (a) neat ASA, (b) ZnO, (c) CaMoO$_4$, (d) Y$_2$O$_3$, (e) TiO$_2$, (f) Sb$_2$O$_3$, (g) BaTiO$_3$.
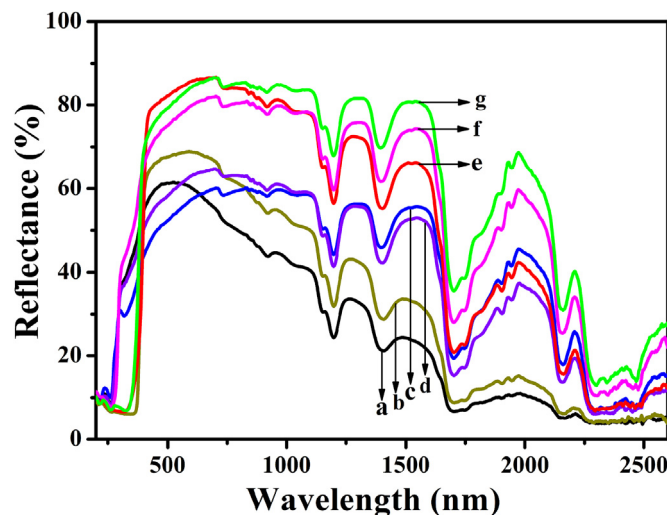

Fig. 6. Solar reflectance of ASA and its hybrid composites: (a) neat ASA, (b) ASA/ZnO, (c) ASA/CaMoO$_4$, (d) ASA/Y$_2$O$_3$, (e) ASA/TiO$_2$, (f) ASA/Sb$_2$O$_3$, (g) ASA/BaTiO$_3$.

The figure reveals that the solar reflectance of all the hybrid composites is higher at visible and near-infrared band compared with neat ASA. This is mainly caused by the high solar reflectance of these inorganic particles as confirmed in Fig. 5.

In order to compare the solar reflectance quantitatively, the irradiance-weighted average reflectance values of ASA and its hybrid composites were calculated according to Eqs. (1)–(2), and the results are displayed in Table 2. As can be seen, in ultraviolet region, the composites containing ZnO, TiO$_2$ and BaTiO$_3$ have much lower reflectance values compared with neat ASA. This is mainly due to the strong ultraviolet absorption ability of these three particles. In visible and near infrared regions, the hybrid composites all show higher reflectance. Since the mid-IR overtones of carbon hydrogen single bond result in a large inevitable absorption of the near infrared light (>1000 nm), the reflectance values in near infrared region is not as much as that in visible region [31].

Then, let's focus on the total solar reflectance values. There is no doubt that the total solar reflectance values of the hybrid composites are all higher than that of neat ASA. Especially, ASA/TiO$_2$, ASA/Sb$_2$O$_3$ and ASA/BaTiO$_3$ these three composites all have much higher reflectance values, which are all above 60%, 1.5 times more than that of neat ASA. As reported in literature, for composites composed of pigments and resins, the solar reflection efficiency relies on the refractive index of pigments and materials with higher refractive index usually possess higher reflectance [32]. The refractive index of TiO$_2$, Sb$_2$O$_3$ and BaTiO$_3$ is 2.7 [33], 2.1 [34] and 2.4 [35], while that of ZnO, CaMoO$_4$ and Y$_2$O$_3$ is approximately 2.0 [36], 1.9 [37] and 1.9 [38], respectively. Therefore, the much higher

Table 2
Detailed irradiance-weighted average reflectance values of ASA and its hybrid composites.

Samples	R_u (%)	R_v (%)	R_n (%)	R_{sol} (%)
ASA	40.86 ± 0.51	59.37 ± 0.87	21.79 ± 0.16	38.90 ± 0.27
ASA/ZnO	12.97 ± 0.20	67.24 ± 0.28	27.82 ± 0.12	44.02 ± 0.14
ASA/CaMoO$_4$	33.29 ± 1.29	54.24 ± 0.32	40.92 ± 0.32	46.27 ± 0.12
ASA/Y$_2$O$_3$	38.91 ± 1.33	59.98 ± 0.64	38.46 ± 0.64	47.73 ± 0.55
ASA/TiO$_2$	14.10 ± 0.10	82.88 ± 0.75	49.01 ± 0.50	61.83 ± 0.56
ASA/Sb$_2$O$_3$	46.06 ± 0.54	76.72 ± 0.60	55.03 ± 0.48	63.91 ± 0.53
ASA/BaTiO$_3$	20.44 ± 0.20	81.01 ± 0.99	61.16 ± 0.73	67.66 ± 0.69

All reflectance values of different bands (R_u, R_v, R_n) were calculated by Eq. (1), the total solar reflectance values R_{sol} was calculated by Eq. (2).

reflectance values of ASA/TiO$_2$, ASA/Sb$_2$O$_3$ and ASA/BaTiO$_3$ may be partially caused by the relatively higher refractive index of those three inorganic pigments. Outstandingly, the composite containing BaTiO$_3$ has the highest value, which is 67.66%, nearly 2 times that of neat ASA. Besides, it can also be found that ASA/BaTiO$_3$ composite could be classified as solar reflective ASA-Π mentioned in design concept section, which indicates an excellent weather resistance and more protection to ASA matrix.

4.2.2. Temperature test

The temperature test is applied to directly reflect the real cooling property of the samples. Fig. 7 shows the results of indoor temperature test. The temperature-rising process can be roughly divided into the following three stages. In the initial 15 min, the internal temperature rises at a relatively fast rate. Afterwards, from 15 to 45 min, the internal temperature rises at a gradually declining rate with the increasing time. Eventually, in the last 15 min, the internal temperature levels off. Obviously, the internal temperature of the device covered with glass increases to the highest, which is around 60 °C, nearly 20 °C higher than that of the device covered with neat ASA. And this is mainly due to direct solar radiation without any obstruction. Besides, compared with neat ASA, all the hybrid composite samples present better cooling effect which can be owing to the addition of the inorganic particles with high solar reflectance. In addition, the temperature differences among ASA/TiO$_2$, ASA/Sb$_2$O$_3$ and ASA/BaTiO$_3$ are quite small as illustrated in Fig. 7 and the remaining three samples present the same trend. On one hand, these small discrepancies are mainly ascribed to the similar solar reflectance values displayed in Table 2. On the other hand, mixing factor also exists during the experiment but is not the major factor. Anyway, the composite containing BaTiO$_3$ still show the best cooling effect, nearly 10 °C lower than neat ASA. In fact, the cooling effect is in highly consistent with the result of solar reflectance.

Apart from the indoor temperature test, the outdoor temperature test was also conducted to support each other. And the results are shown in Fig. 8. It can be seen from the figure that the internal temperature change of the devices tested in the outdoor sunlight shows a same trend with that tested by the solar simulator. The internal temperature of the device covered with glass shows the most significant rise with the increasing time. By comparison, the devices covered with neat ASA and its hybrid composites exhibit
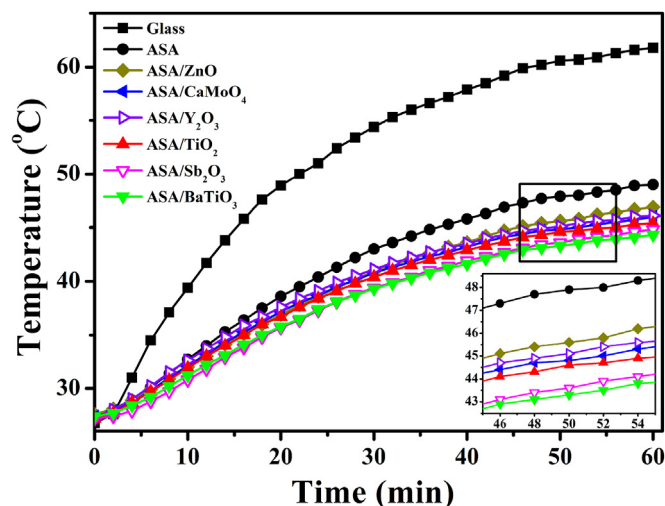

Fig. 8. The temperature change of the inner space of the device versus time interval (outdoor). This temperature test was measured from 12:45—13:45 on 28th July 2016, the real-time temperature of environment was 38 °C, 32°4′37″N, 118°46′19″E, in city Nanjing, China.

much lower internal temperature, indicating that the introduction of inorganic particles can really improve the cooling property of ASA. The only different is that the temperature-rising curves of the outdoor temperature test are denser compared with those of the indoor temperature test. The reasons may be as follows. The conditions of the indoor temperature test were controllable while those of the outdoor temperature test were not. The outdoor temperature test may be influenced by many uncertain factors, including the nondirective winds, the floating clouds, the environmental temperature and the solar irradiance intensity received by the samples. And all these factors were changing all the time.

4.3. Mechanical properties of ASA and its hybrid composites

As is well known, mechanical property is one of the most important performances for materials [39]. Generally, the addition of inorganic particles will affect the mechanical properties of the polymer matrix, which tends to increase the stiffness of the composite but decrease its toughness [40]. For this reason, the mechanical properties were tested to evaluate whether the practical performance of the composites has declined compared with neat ASA. The mechanical properties of ASA and its hybrid composites are illustrated in Fig. 9. The impact strength and elongation at break are usually used to evaluate the toughness of materials. From Fig. 9a and b, it can be found that, compared with control (neat ASA), the toughness of all the hybrid composites almost remains unchanged or slightly higher. This is mainly caused by the following two reasons. One is that the volume fraction of inorganic particles is too low, which is only 1%. Such low volume fraction has little effect on the toughness. The other one is that the small amounts of inorganic particles promote the termination of the crazes and the transfer of stresses and elastic deformations from the ASA matrix to inorganic particles [41]. The remaining three properties usually reflect the stiffness of materials. Certainly, the stiffness of all the hybrid composites increases due to the introduction of the rigid inorganic particles. In conclusion, the addition of the inorganic particles has little effect on the mechanical properties of ASA, indicating that the improvement of the cooling properties is based on no sacrifice of the mechanical properties.
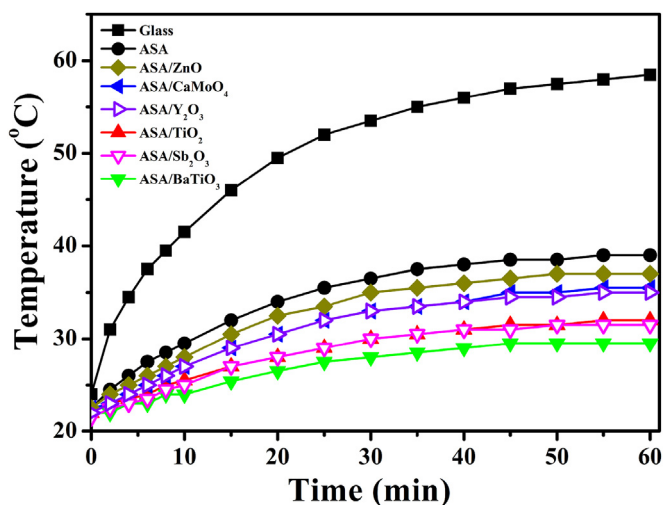

Fig. 7. The temperature change of the inner space of the device versus time interval (indoor). The light intensity at the surface of test sample is 0.3 W/cm^2.
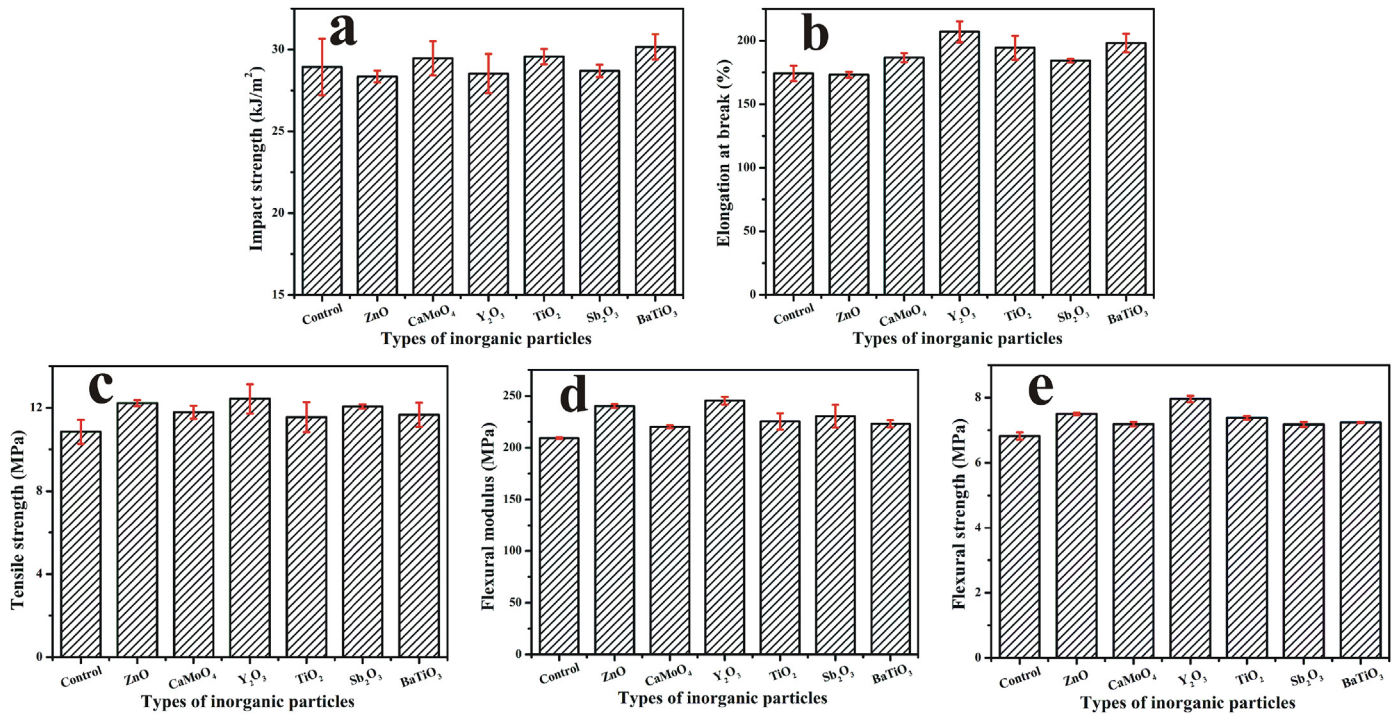
Fig. 9. Mechanical properties of ASA and its hybrid composites: (a) impact strength, (b) elongation at break, (c) tensile strength, (d) flexural modulus, (e) flexural strength.

5. Conclusions

In this study, the concept of solar reflective ASA for cool material was proposed. To achieve this purpose, six kinds of inorganic particles with high solar reflectance were chose to mix with ASA via melt blending to improve the cooling property of ASA. Through a series of analyses and comparison, one can draw the following conclusions. The results of the solar spectral test told that the addition of only 1% volume fraction of inorganic particles could effectively improve the solar reflectance of ASA. And among them, ASA/BaTiO$_3$ hybrid composite possessed the highest reflectance value of 67.66%, nearly 2 times that of neat ASA. The results of the indoor temperature test were in highly consistent with those of the solar reflectance, which showed that all the hybrid composites presented better cooling effect compared with neat ASA. Also, ASA/BaTiO$_3$ hybrid composite exhibited the best cooling effect, nearly 10 °C lower than neat ASA. Besides, the outdoor temperature test showed the same trend with the indoor temperature test. Furthermore, the results of the mechanic test indicated that the improvement of the cooling properties was based on no sacrifice of the mechanical properties.

Acknowledgements

References

[1] G.R. Timilsina, L. Kurdgelashvili, P.A. Narbel, Solar energy: markets, economics and policies, Renew. Sust. Energ. Rev. 16 (1) (2012) 449—465.

[2] G.A.E. Vandenbosch, Z. Ma, Upper bounds for the solar energy harvesting efficiency of nano-antennas, Nano Energy 1 (3) (2012) 494—502.

[3] S.A. Kim, S.J. Yun, S.H. Lee, I.G. Hwang, M.S. Rhee, Temperature increase of foods in car trunk and the potential hazard for microbial growth, Food Control. 29 (1) (2013) 66—70.

[4] R. Qi, L. Lu, H. Yang, Investigation on air-conditioning load profile and energy consumption of desiccant cooling system for commercial buildings in Hong Kong, Energ. Build. 49 (2) (2012) 509—518.

[5] J. Song, J. Qin, J. Qu, Z. Song, W. Zhang, X. Xue, Y. Shi, T. Zhang, W. Ji, R. Zhang, The effects of particle size distribution on the optical properties of titanium dioxide rutile pigments and their applications in cool non-white coatings, Sol. Energ. Mat. Sol. C 130 (2014) 42—50.

[6] S. Soumya, A.P. Mohamed, L. Paul, K. Mohan, S. Ananthakumar, Near IR reflectance characteristics of PMMA/ZnO nanocomposites for solar thermal control interface films, Sol. Energ. Mat. Sol. C 125 (125) (2014) 102—112.

[7] A.K.V. Raj, P.P. Rao, S. Sameera, S. Divya, Pigments based on terbium-doped yttrium cerate with high NIR reflectance for cool roof and surface coating applications, Dyes Pigm. 122 (2015) 116—125.

[8] S. Lu, Y. Chen, S. Liu, X. Kong, Experimental research on a novel energy efficiency roof coupled with PCM and cool materials, Energ. Build. 127 (2016) 159—169.

[9] Y.L. Liang, E. Moghbelli, H.J. Sue, R. Minkwitz, R. Stark, Effect of high temperature annealing on scratch behavior of acrylonitrile styrene acrylate copolymers, Polymer 53 (2) (2012) 604—612.

[10] J.S. Bloom, J.D. Connolly, Polymer-based products having improved solar reflectivity and UV protection, US 20110151163 A1, 2011.

[11] X. Gao, J. Li, Y. Gao, S. Guo, H. Wu, R. Chen, Microwave absorbing properties of alternating multilayer composites consisting of poly (vinyl chloride) and multi-walled carbon nanotube filled poly (vinyl chloride) layers, Compos. Sci. Technol. 130 (2016) 10—19.

[12] L. Zuo, W. Fan, Y. Zhang, L. Zhang, W. Gao, Y. Huang, T. Liu, Graphene/montmorillonite hybrid synergistically reinforced polyimide composite aerogels with enhanced flame-retardant performance, Compos. Sci. Technol. 139 (2017) 57—63.

[13] S. Wang, J. Zhang, Effect of titanium dioxide (TiO$_2$) on largely improving solar reflectance and cooling property of high density polyethylene (HDPE) by influencing its crystallization behavior, J. Alloy. Compd. 617 (1) (2014) 163—169.

[14] Y. Li, J. Yuan, J. Xue, F. Cai, F. Chen, Q. Fu, Towards suppressing loss tangent: effect of polydopamine coating layers on dielectric properties of core-shell barium titanate filled polyvinylidene fluoride composites, Compos. Sci. Technol. 118 (2015) 198—206.

[15] H. Tang, P. Wang, P. Zheng, X. Liu, Core-shell structured BaTiO$_3$@polymer hybrid nanofiller for poly(arylene ether nitrile) nanocomposites with enhanced dielectric properties and high thermal stability, Compos. Sci. Technol. 123 (2016) 134—142.

[16] P. Katangur, P.K. Patra, S.B. Warner, Nanostructured ultraviolet resistant polymer coatings, Polym. Degrad. Stabil. 91 (10) (2006) 2437—2442.

[17] R. Levinson, P. Berdahl, H. Akbari, W. Miller, I. Joedicke, J. Reilly, Y. Suzuki, M. Vondran, Methods of creating solar-reflective nonwhite surfaces and their

application to residential roofing materials, Sol. Energ. Mater. Sol. C 91 (4) (2007) 304–314.

[18] B. Xiang, Y. Qi, S. Wang, J. Zhang, Using a novel and easy-to-use sandwich structure device to evaluate the cooling properties of cool materials, Int. J. Polym. Anal. Charact. 20 (6) (2015) 529–540.

[19] L. Fang, W. Wu, X. Huang, J. He, P. Jiang, Hydrangea-like zinc oxide super-structures for ferroelectric polymer composites with high thermal conductivity and high dielectric constant, Compos. Sci. Technol. 107 (2015) 67–74.

[20] X. Li, Z. Yang, L. Guan, J. Guo, Y. Wang, Q. Guo, Synthesis and luminescent properties of $CaMoO_4$: Tb^{3+}, R^+ (Li^+, Na^+, K^+), J. Alloy. Compd. 478 (1–2) (2009) 684–686.

[21] L. Qiang, Y. Wu, L. Ding, G. Zu, A. Li, Y. Zhao, H. Cui, Visible upconversion luminescence of Tb^{3+} ions in Y_2O_3 nanoparticles induced by a near-infrared femtosecond laser, J. Alloy. Compd. 496 (1–2) (2010) 488–493.

[22] M. Zhen, X. Guo, G. Gao, Z. Zhou, L. Liu, Rutile TiO_2 nanobundles on reduced graphene oxides as anode materials for Li ion batteries, Chem. Commun. 50 (80) (2014) 11915–11918.

[23] A. Khan, M. Saleemi, M. Johnsson, L. Han, N.V. Nong, M. Muhammed, M.S. Toprak, Fabrication, spark plasma consolidation, and thermoelectric evaluation of nanostructured $CoSb_3$, J. Alloy. Compd. 612 (5) (2014) 293–300.

[24] D.Y. Lu, Y.Y. Peng, Dielectric properties and exploration of self-compensation mode of Tb in $BaTiO_3$ ceramics, J. Ceram. Soc. Jpn. 124 (4) (2016) 455–459.

[25] S. Musić, S. Popović, M. Maljković, Đ. Dragčević, Influence of synthesis procedure on the formation and properties of zinc oxide, J. Alloy. Compd. 347 (1) (2002) 324–332.

[26] A.A. Ansari, A.K. Parchur, M. Alam, J. Labis, A. Azzeer, Influence of surface coating on structural and photoluminescent properties of $CaMoO_4$: Pr nano-particles, J. Fluoresc. 24 (4) (2014) 1253–1262.

[27] N.J. Shivaramu, B.N. Lakshminarasappa, K.R. Nagabhushana, F. Singh, Luminescence studies of 100MeV Si^{8+} ion irradiated nanocrystalline Y_2O_3, Radiat. Meas. 71 (1) (2014) 518–523.

[28] X. Tian, K. He, C. Wang, Q. Wen, B. Wang, S. Yu, C. Hao, K. Chen, Q. Lei, Preparation and electrorheological behavior of anisotropic titanium oxide/polyaniline core/shell nanocomposite, Compos. Sci. Technol. 137 (2016) 118–129.

[29] M. Nalin, Y. Messaddeq, S.J.L. Ribeiro, M. Poulain, V. Briois, G. Brunklaus, C. Rosenhahn, B.D. Mosel, H. Eckert, Structural organization and thermal properties of the Sb_2O_3-$SbPO_4$ glass system, J. Mater. Chem. 14 (23) (2004) 3398–3405.

[30] N.R. Alluri, S. Selvarajan, A. Chandrasekhar, B. Saravanakumar, J.H. Jeong, S.-J. Kim, Piezoelectric $BaTiO_3$/alginate spherical composite beads for energy harvesting and self-powered wearable flexion sensor, Compos. Sci. Technol. 142 (2017) 65–78.

[31] G. Oreski, D. Tscharnuter, G.M. Wallner, Determination of solar optical properties of transparent polymer films using UV/vis spectroscopy, Sol. Energ. Mater. Sol. C 94 (5) (2010) 884–891.

[32] G. Buxbaum, G. Pfaff, Industrial Inorganic Pigments, third ed., Wiley-VCH, Weinheim, 2005.

[33] M.R. Mohammadi, A.M. Bakhshayesh, F. Sadri, M. Masroor, Improved efficiency of dye-sensitized solar cells by design of a proper double layer photoanode electrodes composed of Cr-doped TiO_2 transparent and light scattering layers, J. Sol. Gel. Sci. Technol. 67 (1) (2013) 77–87.

[34] O.E.L. Pérez, M.A. Pérez, M.L. Teijelo, Characterization of the anodic growth and dissolution of antimony oxide films, J. Electroanal. Chem. 632 (1–2) (2009) 64–71.

[35] D.K. Patel, B. Vishwanadh, V. Sudarsan, S.K. Kulshreshtha, Difference in the nature of Eu^{3+} environment in Eu^{3+}-Doped $BaTiO_3$ and $BaSnO_3$, J. Am. Ceram. Soc. 96 (12) (2013) 3857–3861.

[36] T. Minemoto, T. Mizuta, H. Takakura, Y. Hamakawa, Antireflective coating fabricated by chemical deposition of ZnO for spherical Si solar cells, Sol. Energ. Mat. Sol. C 91 (2) (2007) 191–194.

[37] Z. Khadraoui, K. Horchani-Naifer, M. Ferhi, M. Ferid, Synthesis, characterization and DFT calculations of electronic and optical properties of $YbPO_4$, Chem. Phys. 457 (2015) 37–42.

[38] S.H. Im, D.H. Jin, J.P. Kim, Y.J. Hong, S.H. Lee, Siloxane based coating composition having excellent dyeabililty abrasion resistance, glossiness and transparency, and a preparation method thereof, and an optical lens coated by said coating composition, US 20100064939 A1, 2010.

[39] J.Z. Liang, Reinforcement and quantitative description of inorganic particulate-filled polymer composites, Compos. Part B Eng. 51 (4) (2013) 224–232.

[40] L. Nicolais, M. Narkis, Stress-strain behavior of styrene-acrylonitrile/glass bead composites in the glassy region, Polym. Eng. Sci. 11 (11) (1971) 194–199.

[41] P. Carballeira, F. Haupert, Toughening effects of titanium dioxide nanoparticles on TiO_2/epoxy resin nanocomposites, Polym. Compos. 31 (7) (2010) 1241–1246.